Supporting Information for
"A revised look at relativistic electrons in the Earth's inner radiation zone and slot region"

S. G. Claudepierre[1,2], T. P. O'Brien[1], M. D. Looper[1], J. B. Blake[1], J. F. Fennell[1], J. L. Roeder[1], J. H. Clemmons[3], J. E. Mazur[1], D. L. Turner[1], G. D. Reeves [4], and H. E. Spence[3]

[1]Space Sciences Department, The Aerospace Corporation, El Segundo, California, USA
[2]Department of Atmospheric and Oceanic Sciences, UCLA, Los Angeles, California, USA
[3]Institute for the Study of Earth, Oceans, and Space, University of New Hampshire, Durham, New Hampshire, USA
[4]Space and Atmospheric Sciences Group, Los Alamos National Laboratory, Los Alamos, New Mexico, USA

Contents

1. Figures S1 to S8
2. Table S1

Additional Supporting Information (Files uploaded separately)

1. Data Set S1

Introduction

This Supporting Information is meant to supplement the exposition provided in the main manuscript and to describe the CDF data file that is provided. Please refer to the captions for Figure S1 - Figure S8 and to the main manuscript for more details.

Data Set S1.

A Common Data Format (CDF) data file is provided that contains the three flux variables used in the main manuscript: The uncorrected flux (UNCORR), the standard background-corrected flux (CORR-STD), and the alternative background-corrected flux (CORR-ALT). The fluxes in the CDF file are daily averages, binned in McIlwain L from $L = [1.0, 7.6]$ in $\Delta L = 0.1$ bins. The Olson and Pfitzer (1977) quiet magnetic field model is used. The fluxes are computed near the magnetic equator when $B/B_{eq} \leq 1.1$, where B/B_{eq} is the ratio of the magnetic field strength at the spacecraft to that at the magnetic equator (both obtained from the model). The fluxes are averaged around 90 degrees local pitch angle ($\alpha_L = [80, 100]$ degrees) which, for this B/B_{eq} range, corresponds to equatorial pitch angles between 70 and 110 degrees.

There are three flux variables in the CDF file:

1. **FEDU**: Uncorrected, unidirectional, differential electron flux, with units $(\text{cm}^2 \text{ s sr keV})^{-1}$. This is the "UNCORR" data from the manuscript.
2. **FEDU_CORR**: Background-corrected (standard algorithm), unidirectional, differential electron flux, with units $(\text{cm}^2 \text{ s sr keV})^{-1}$. This is the "CORR-STD" data from the manuscript.

Corresponding author: S. G. Claudepierre, `sethclaudepierre@gmail.com`
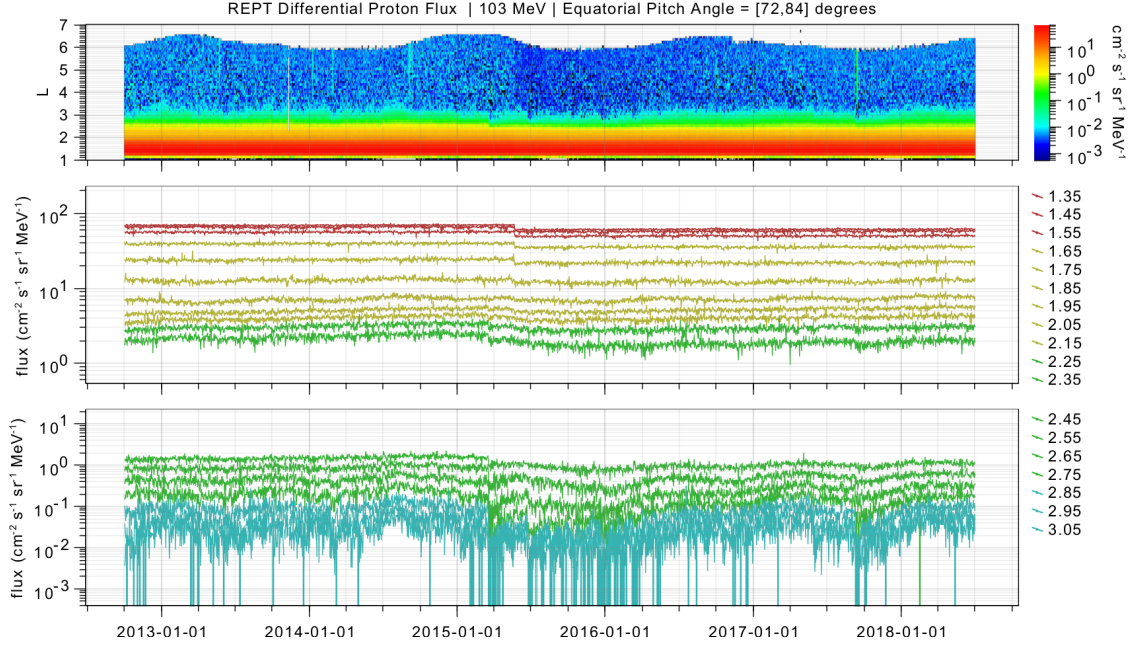
Figure S1. Van Allen Probes REPT (Baker et al., 2013) observations demonstrating that 100 MeV proton fluxes are stable to within a factor of ∼2 in the heart of the inner belt ($L = [1.3,2.4]$) over the course of the mission to date. The top panel shows 100 MeV proton fluxes in L versus time format for equatorial pitch angles between 72 and 84 degrees. The middle panel shows slices in L through the heart of the inner belt ($L = [1.3,2.4]$). Similar stability is observed at other equatorial pitch angles, and at higher energies from the RPS instrument (not shown here). Note also that there is no sporadic enhancement of the inner proton belt observed near $L = 1.5$ (or any other L) in May of 2017 (see main manuscript for a discussion of the May 2017 inner zone electron enhancement). The bottom panel shows slices at the outer edge of the inner proton belt ($L = [2.5,3.1]$) where the fluxes are more variable.

3. **FEDU_CORR_ALT**: Background corrected (alternative algorithm), unidirectional, differential electron flux, with units $(cm^2 \ s \ sr \ keV)^{-1}$. This is the "CORR-ALT" data from the manuscript.

All of the flux arrays in the CDF file are ∼ [*ntime* x *nenergy* x *nL*] in array size. Here, *ntime* = 1826, the number of time points; *nenergy* = 21, the number of energy channels; and *nL* = 66, the number of L bins. All available MagEIS energy channels are provided, 30 keV - 4 MeV, from the LOW, M75, and HIGH units (LOW P0-P1 and M75 P0-P1 are noisy and are not provided). The energy channels are displayed in Table S1. As described in the manuscript, the CORR-ALT data is only computed at energies greater than 700 keV and only for at $L \leq 3$, so that it is a merged data product: For all energies below 700 keV, the CORR-ALT data is identical to the CORR-STD data at all L; and for $L > 3$ and energies above 700 keV, the CORR-ALT data is identical to the CORR-STD data. The CORR-ALT data is only different from the CORR-STD data for $L \leq 3$ and energies greater than 700 keV, where the alternative algorithm is used instead of the standard algorithm.
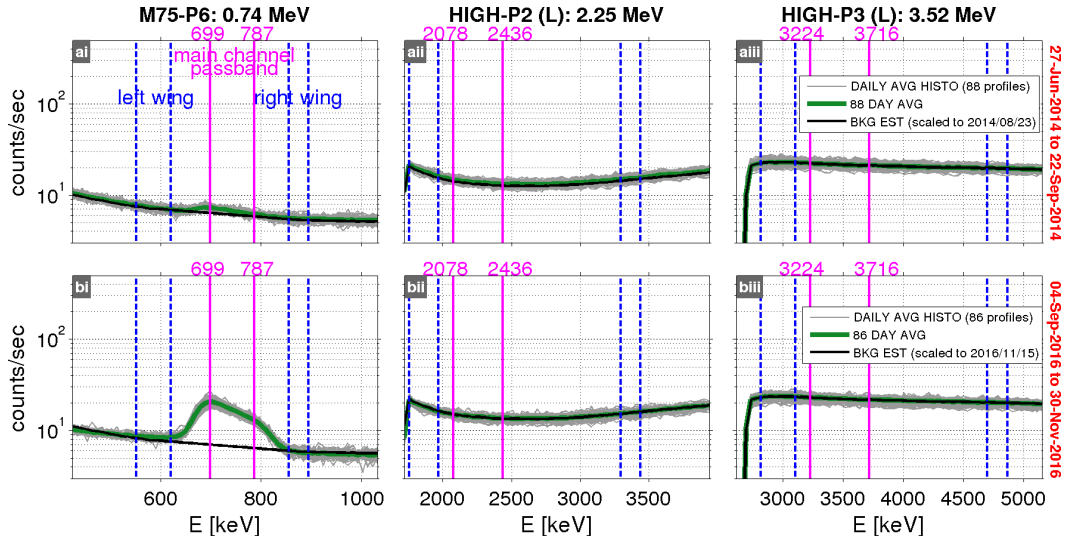
Figure S2. Figure analogous to Figure 2 in the main manuscript, but here showing the three other pixels under consideration: M75-P6, HIGH-P2 (left channel shown), and HIGH-P3 (left channel shown). Note that there is a gap in energy between panels ai/bi (0.74 MeV) and the subsequent panels (2.25 MeV, 3.52 MeV). Also note that the background estimate for M75-P6 is interpolated from the left wing to the right wing, as described in Appendix A in the main manuscript (note the small passband peak in panel ai, green).

References

Baker, D. N., Kanekal, S. G., Hoxie, V. C., Batiste, S., Bolton, M., Li, X., ... Friedel, R. (2013, November). The Relativistic Electron-Proton Telescope (REPT) Instrument on Board the Radiation Belt Storm Probes (RBSP) Spacecraft: Characterization of Earth's Radiation Belt High-Energy Particle Populations. *Space Sci. Rev.*, *179*, 337-381. doi: 10.1007/s11214-012-9950-9

Claudepierre, S. G., O'Brien, T. P., Blake, J. B., Fennell, J. F., Roeder, J. L., Clemmons, J. H., ... Larsen, B. A. (2015, July). A background correction algorithm for Van Allen Probes MagEIS electron flux measurements. *J. Geophys. Res.*, *120*, 5703-5727. doi: 10.1002/2015JA021171

Olson, W. P., & Pfitzer, K. A. (1977, January). *Magnetospheric magnetic field modeling* (Tech. Rep. No. Annual Report). Huntington Beach, CA.: McDonnell-Douglas Astronautics Co.
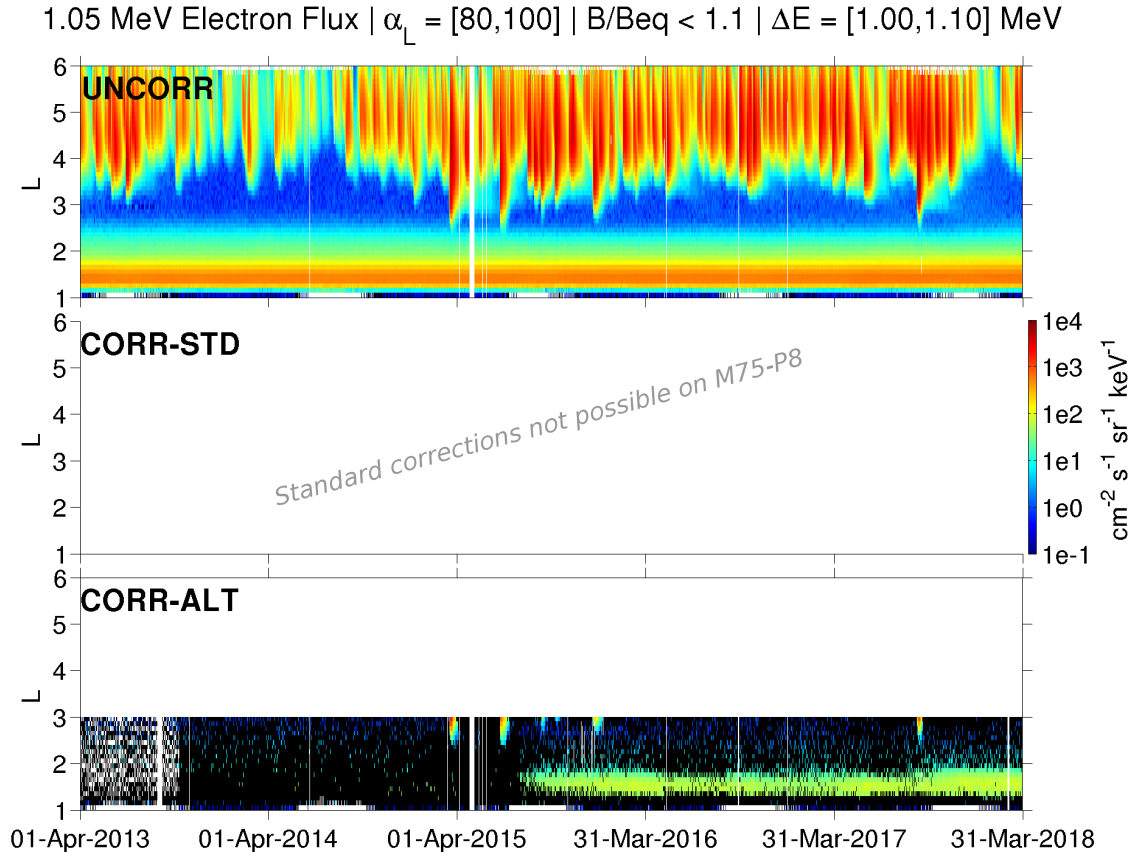
Figure S3. Same format as Figures 3-6 in the main manuscript but for 1.05 MeV electrons (M75-P8). Note that the CORR-ALT data from this channel from M75-P8 should be used with an abundance of caution, due to poor counting statistics. The HIGH-P0 channel has a similar centroid energy and should be used instead. There is no CORR-STD data (or CORR-ALT data above $L = 3$) because the standard background corrections are not possible on this pixel (see Claudepierre et al. (2015)). In addition, for M75-P8, we note that the alternative algorithm scales to the left wing rather than the right wing, due to the fact that the right wing is undefined for this pixel (see main manuscript for a description of the scaling).
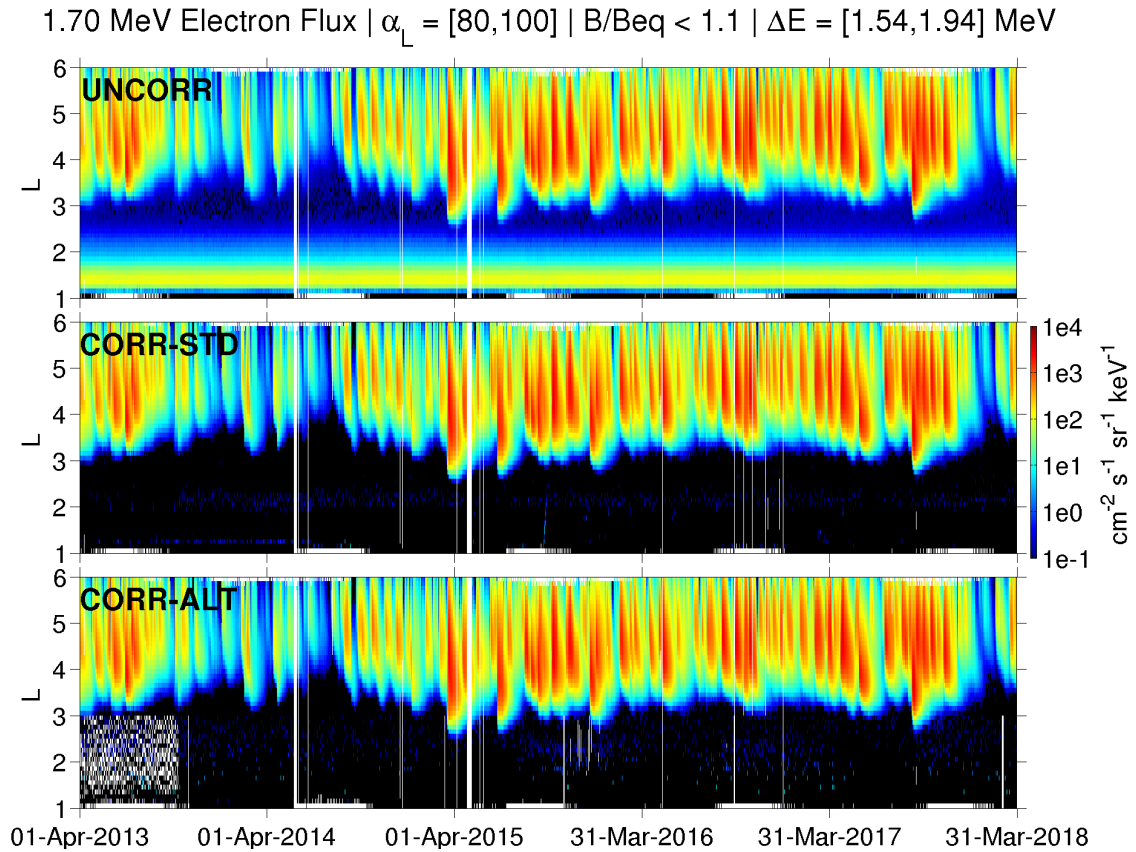
Figure S4. Same format as Figures 3-6 in the main manuscript but for 1.70 MeV electrons (HIGH-P1, right channel). Note in the CORR-ALT data that no electrons are observed in the inner zone. There is faint residual contamination in the inner zone that is not entirely removed by the background correction algorithm, but this is spurious and not real foreground signal (see main manuscript).
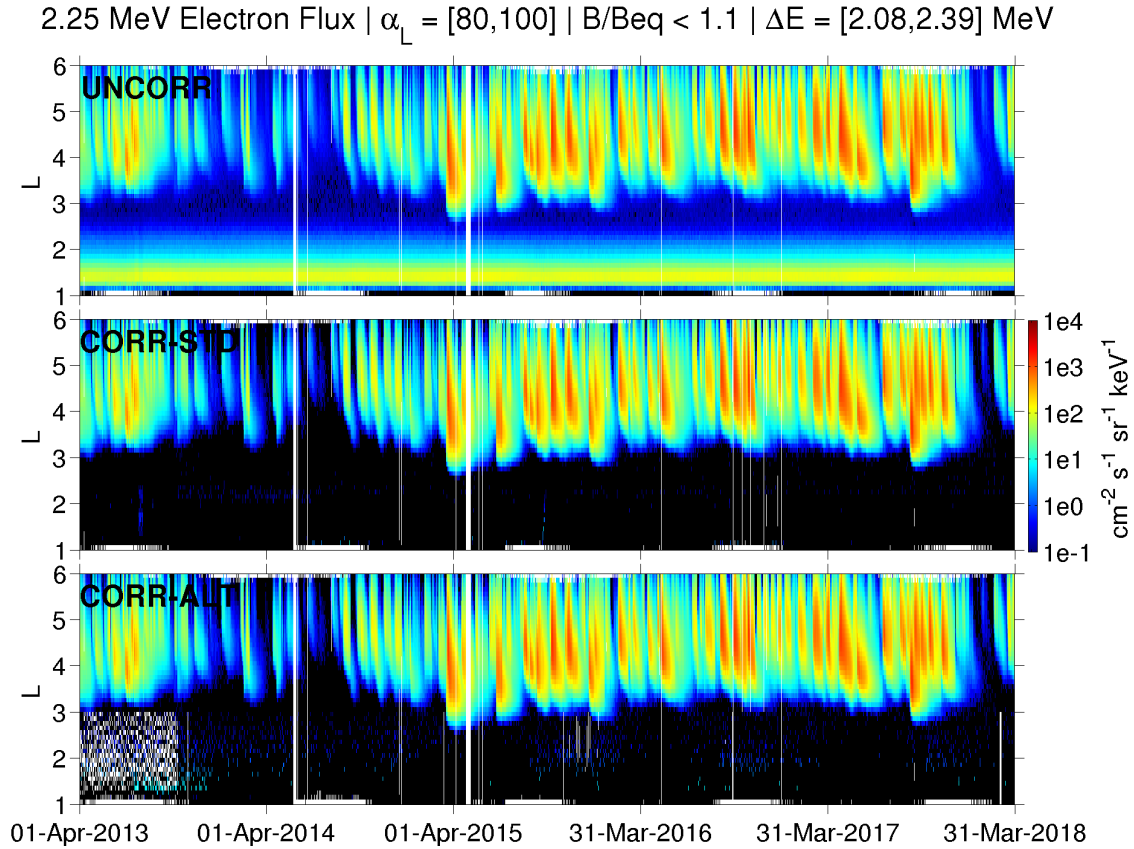
Figure S5. Same format as Figures 3-6 in the main manuscript but for 2.25 MeV electrons (HIGH-P2, left channel). Note in the CORR-ALT data that no electrons are observed in the inner zone. There is faint residual contamination in the inner zone that is not entirely removed by the background correction algorithm, but this is spurious and not real foreground signal (see main manuscript).
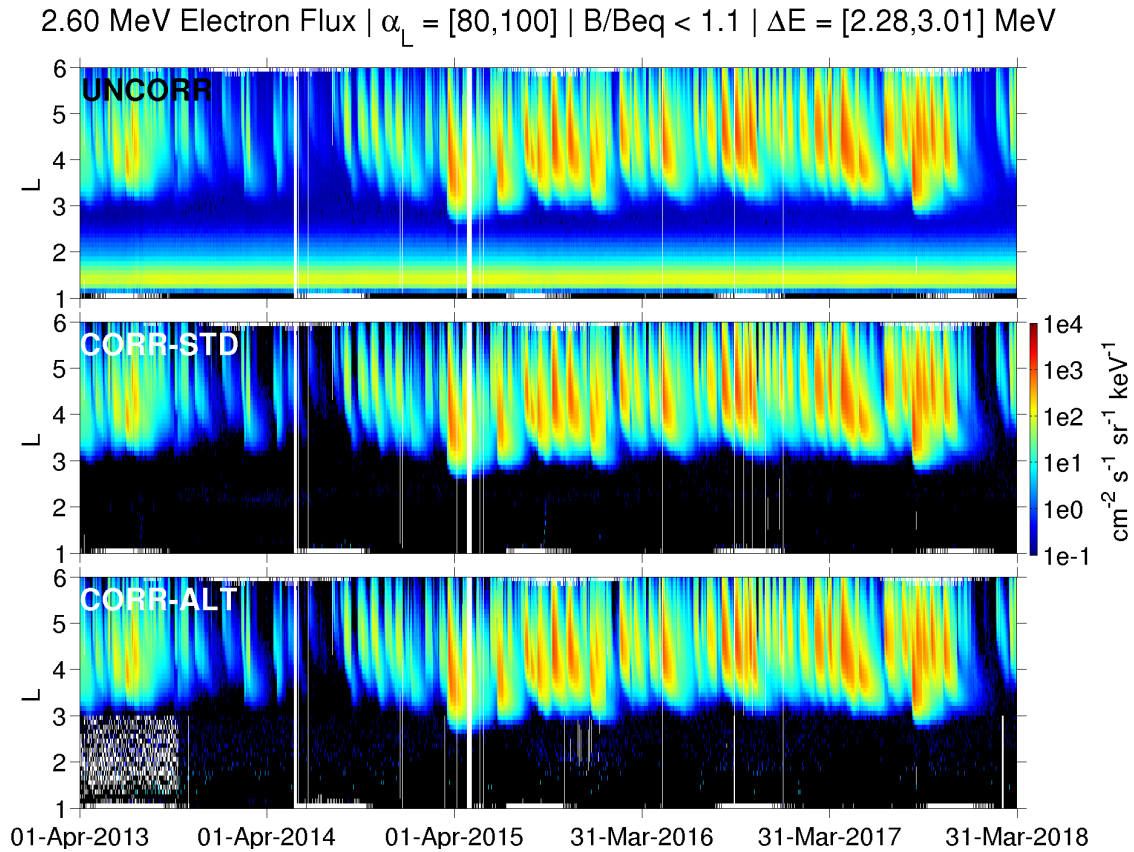
Figure S6. Same format as Figures 3-6 in the main manuscript but for 2.60 MeV electrons (HIGH-P2, right channel). Note in the CORR-ALT data that no electrons are observed in the inner zone. There is faint residual contamination in the inner zone that is not entirely removed by the background correction algorithm, but this is spurious and not real foreground signal (see main manuscript).
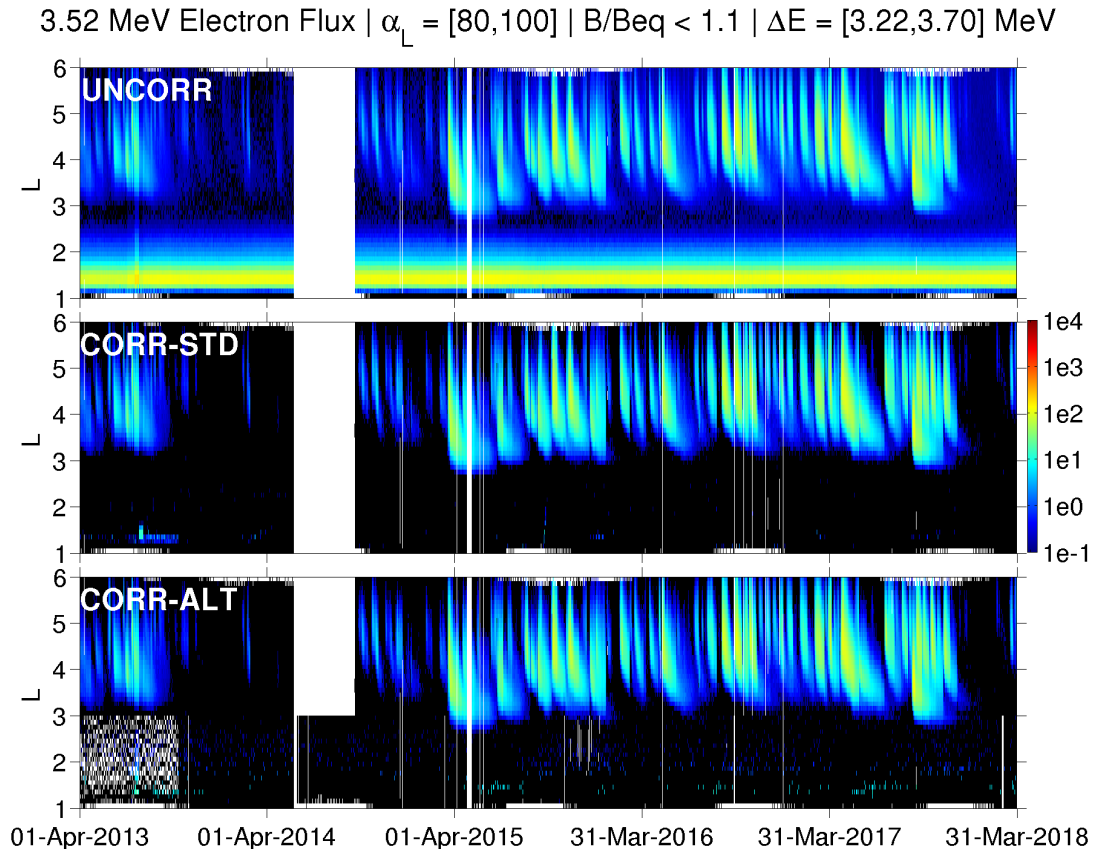
Figure S7. Same format as Figures 3-6 in the main manuscript but for 3.52 MeV electrons (HIGH-P3, left channel). Note in the CORR-ALT data that no electrons are observed in the inner zone. There is faint residual contamination in the inner zone that is not entirely removed by the background correction algorithm, but this is spurious and not real foreground signal (see main manuscript).
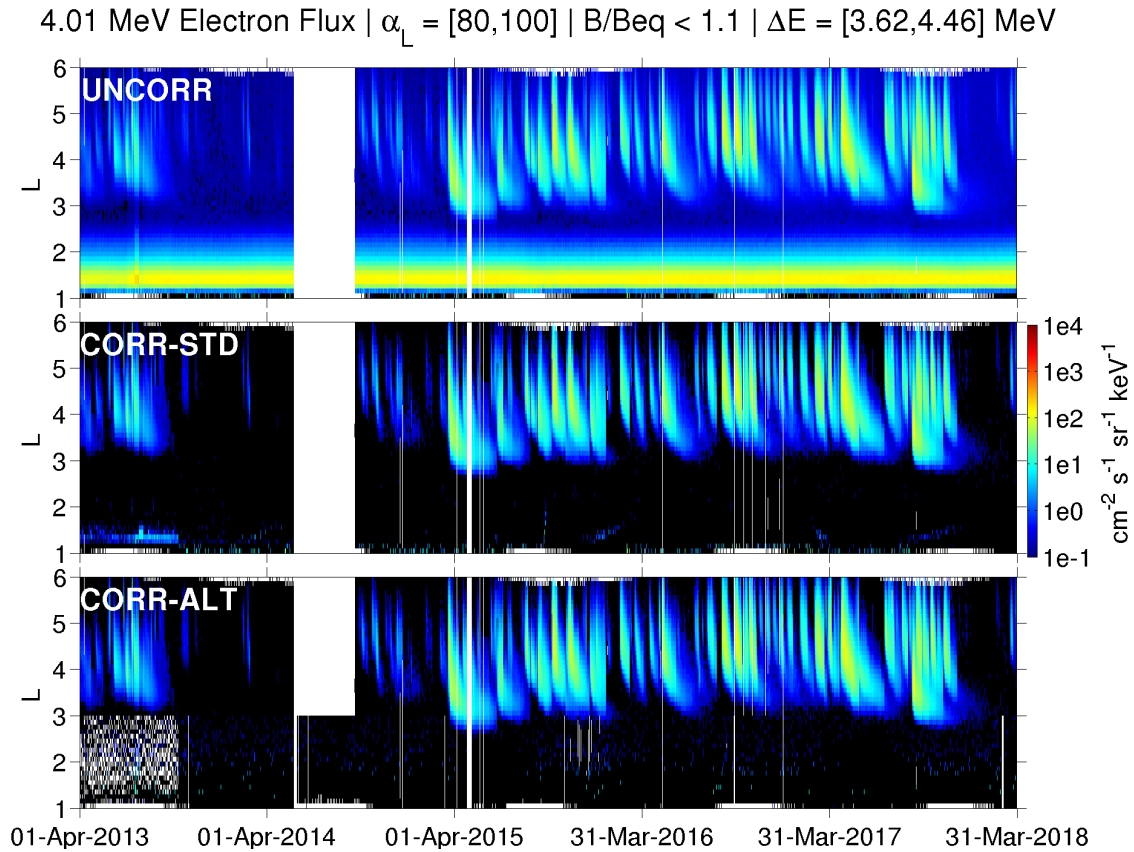
Figure S8. Same format as Figures 3-6 in the main manuscript but for 4.01 MeV electrons (HIGH-P3, right channel). Note in the CORR-ALT data that no electrons are observed in the inner zone. There is faint residual contamination in the inner zone that is not entirely removed by the background correction algorithm, but this is spurious and not real foreground signal (see main manuscript).

Table S1. MagEIS Energy Channel Information for the CDF File

Array Index	Energy Channel [keV]	Unit/Pixel #	Channel Passband [keV]	Channel Width [keV]
0	32	LOW-P2	26 - 38	11
1	54	LOW-P3	48 - 61	12
2	75	LOW-P4	69 - 81	12
3	102	LOW-P5	95 - 108	13
4	132	LOW-P6	124 - 141	18
5	169	LOW-P7	158 - 180	22
6	210	LOW-P8	196 - 224	28
7	242	M75-P2	222 - 262	40
8	350	M75-P3	317 - 382	65
9	467	M75-P4	431 - 503	73
10	600	M75-P5	565 - 635	70
11	743	M75-P6	699 - 787	88
12	892	M75-P7	843 - 941	99
13	1013	HIGH-P0	970 - 1279	309
14[a]	1050[a]	M75-P8[a]	995 - 1104[a]	109[a]
15	1541	HIGH-P1 (L)	1403 - 1728	325
16	1704	HIGH-P1 (R)	1539 - 1939	400
17	2249	HIGH-P2 (L)	2078 - 2387	309
18	2596	HIGH-P2 (R)	2280 - 3008	728
19	3519	HIGH-P3 (L)	3224 - 3703	479
20	4009	HIGH-P3 (R)	3618 - 4455	837

[a]The channel from M75-P8 should be used with an abundance of caution, due to poor counting statistics.